Model for Fires with Low Initial Momentum and Nongray Thermal Radiation

D. C. WILCOX*

DCW Industries, Sherman Oaks, Calif.

A theoretical fire model has been developed for turbulent diffusion flames having low initial momentum and nongray thermal radiation. Equations of motion are solved using the Kármán-Pohlhausen integral method. To apply the integral method to fires having low initial momentum, a newly postulated ambient-air entrainment law accounts for rapid fluid acceleration from initially low velocity at a liquid pool, to much higher velocities established under buoyant rise of the combustion products. The fire is assumed optically thick in the direction of its symmetry axis, and axial-radiation heat transfer is neglected. In the radial direction, radiation mean free path is assumed finite; radial-radiation heat transfer is computed with the exact radiation transport equation, with all the fire's radiating gaseous species represented as realistic nongray radiators. Fire-model predictions fall within scatter of experimental flame-height and spectral-radiation data for liquefied-natural-gas fires.

I. Introduction

SEVERAL models have been developed to predict properties of large turbulent diffusion flames[1-8]; such fire models generally use an ambient-air entrainment law similar to the one postulated by Taylor, et al.[1] Provided the fire's initial momentum is high enough, such models accurately predict gross fire properties such as flame height and average temperature. To varying degrees, effects of thermal radiation have been included in some models[3,5,7,8]; in these models (with the exception of Wilcox's[8]) the flame is treated as a gray-body radiator, an approximation applicable only to sooty fires. Since, however, many fires of practical interest have low initial momentum (e.g., pool fires) and/or very little soot (e.g., fires with clean-burning fuels such as natural gas), a different model is needed.

This paper describes an improved version of the Wilcox diffusion-flame model encompassing properties of a clean-burning fire with low initial momentum; for simplicity, an idealized natural-gas burning reaction is used in formulating the model. A newly formulated fluid entrainment law improves the Wilcox model. At short distances from a low-momentum fuel source the new law allows for entrainment of much more ambient air than the Taylor law. Once the flame gases have gained sufficient momentum, the new entrainment law displays an asymptotic approach to the Taylor law. No changes to the original Wilcox fire model have been made in treating thermal radiation. As in the original model, the flame is assumed optically thick in the direction of its symmetry axis, and radiative transfer is neglected in the axial direction; the Kármán-Pohlhausen integral method solves the exact radiation-transport equation, and Edwards' exponential-band model[9] is used to represent radiating gases as realistic nongray radiators. Section II gives details of model formulation, and Sec. III applies the model to fires above liquefied-natural-gas (LNG) pools and compares computed results with experimental data. Section IV summarizes conclusions.

II. Model Formulation

The flame is assumed axisymmetric with zero mean swirl. Standard diffusion-flame approximations are made, i.e., axial diffusion is neglected and pressure is assumed constant in flame cross sections. Cylindrical polar coordinates (r, θ, z) are used with corresponding velocity components (u, v, w). The Kármán-Pohlhausen integral method[10] is used; the first step in implementing the method is to integrate the conservation-of-mass, species, momentum, and energy equations over flame cross section; respectively, the resulting equations are

$$d/dz \int_0^\infty \rho w r\, dr = -\lim_{r\to\infty} \rho u r \tag{1}$$

$$d/dz \int_0^\infty \rho w (y^i - y_\infty{}^i) r\, dr = \int_0^\infty P_i r\, dr \tag{2}$$

$$d/dz \int_0^\infty \rho w^2 r\, dr = g \int_0^\infty (\rho_\infty - \rho) r\, dr \tag{3}$$

$$d/dz \int_0^\infty \rho w [h + 1/2 w^2] r\, dr = \int_0^\infty Q_R r\, dr - g \int_0^\infty \rho w r\, dr + h_\infty\, d/dz \int_0^\infty \rho w r\, dr \tag{4}$$

where ρ, h, g, Q_R, y^i, and P_i denote density, enthalpy, gravitational acceleration, radiation heat loss, mass fraction, and chemical production, respectively; subscript ∞ signifies ambient conditions; subscript and superscript i denotes the ith gas. Since flame gases are assumed perfect, the equation of state is

$$\rho T/M = \rho_\infty T_\infty / M_\infty \tag{5}$$

with

$$1/M = \sum_i y^i / M_i \tag{6}$$

where M and T are molecular weight and temperature respectively. Enthalpy is given by

$$h = \sum_i y^i [C_{p_i} (T - T_c) + h_i{}^{(o)}] \tag{7}$$

where T_c is a reference temperature and $h_i{}^{(o)}$ and C_{p_i} denote heat of formation and (constant) specific heat of the ith gas.

By introducing the scaled, nondimensional radial variable, η, defined by the relation

$$\rho r\, dr = \rho_\infty \delta^2 \eta\, d\eta \tag{8}$$

where $\delta(z)$ has the dimension of a length, and by then assuming a top-hat profile for the axial velocity, i.e.,

$$w(\eta, z) = w_o(z) H(1 - \eta) \tag{9}$$

where $H(x)$ is the Heaviside stepfunction, Eqs. (1–4) simplify to

$$d/dz [\rho_\infty w_o \delta^2] = -2 \lim_{r\to\infty} \rho u r \tag{10}$$

$$d/dz [\rho_\infty w_o \delta^2 \int_0^1 (y^i - y_\infty{}^i) \eta\, d\eta] = \int_0^\infty P_i r\, dr \tag{11}$$

$$d/dz [\rho_\infty w_o{}^2 \delta^2] = 2 \rho_\infty g [\bar{\delta}^2 - \delta^2] \tag{12}$$

$$d/dz [2 \int_0^\infty \rho w h r\, dr + 1/2 \rho_\infty w_o{}^3 \delta^2] = 2 \int_0^\infty Q_R r\, dr - \rho_\infty g w_o \delta^2 + h_\infty\, d/dz [\rho_\infty w_o \delta^2] \tag{13}$$

Received March 18, 1974; revision received September 5, 1974.

Index categories: Boundary Layers and Convective Heat Transfer—Turbulent; Reactive Flows.

* Owner; Member AIAA.

where $\hat{\delta}$ is the fire plume radius (i.e., radius at which $w/w_o = 0.01$) related to the scaled radius, δ, by

$$\hat{\delta}^2 = 2\delta^2 \int_0^1 (\rho_\infty/\rho)\eta \, d\eta \tag{14}$$

Additional information is needed to close equation set (5-14). First, to relate $\lim_{r\to\infty} \rho u r$ to the quantities ρ_∞, w_o, δ, etc, an entrainment law must be postulated. Second, so that Eq. (11) can be reduced to an ordinary differential equation, mass-fraction and chemical-production profiles must be specified. Third, to relate $\hat{\delta}$ and δ and to permit evaluation of the enthalpy integral in Eq. (13), a density profile must be prescribed. Finally, to reduce Eq. (13) to an ordinary differential equation, the radiation-heat-loss term must be evaluated. Each of these points is discussed in the following sections.

A. Entrainment Law

Consider first an ambient-fluid entrainment law appropriate for a diffusion flame with a small amount of initial momentum (e.g., a pool fire). Taylor[1] has postulated the simplest entrainment law for weakly buoyant plumes; in terms of present notation, the Taylor law is:

$$-\lim_{r\to\infty} \rho u r = \alpha \rho_\infty w_o \hat{\delta} \tag{15}$$

where α is a constant of order 10^{-1}. For strongly buoyant plumes, such as fire plumes, entrainment depends upon mean plume density, ρ_o; Morton,[5] for example, postulates that for plumes with large density variation, Eq. (15) should be replaced by

$$-\lim_{r\to\infty} \rho u r = \alpha[\rho_o/\rho_\infty]^n \rho_\infty w_o \hat{\delta} \tag{16}$$

with a typical value for n of $\frac{1}{2}$. Both Eqs. (15) and (16) predict that entrainment decreases proportionally with decreasing axial velocity. Hence, for pool fires, for which w_o will be initially small, use of Eq. (15) or (16) leads to prediction of very little entrainment near the pool surface. However, experiments of Thomas et al,[6] indicate vigorous entrainment occurs close to the fuel source for alcohol and town-gas fires; in fact, horizontal inflow velocity achieves its maximum value just above an alcohol pool and decreases monotonically with altitude. Hence, neither the Taylor law Eq. (15) nor the Morton law Eq. (16) appears valid for fires with low initial momentum.

For fire plumes in which w_o is initially small, failure of the Taylor and Morton entrainment laws appears to be due to the assumption that entrainment velocity scales with w_o close to the fuel source. This assumption takes no account of combustion processes which cause rapid local variation in axial velocity; i.e., axial velocity is much higher than the average plume velocity, w_o, near the combustion region and changes very rapidly with increasing altitude. A more appropriate velocity scale would be $r_c \, dw_o/dz$ where r_c is the value of r on the surface where combustion occurs (see Sec. 2B for definition of combustion surface); this velocity scale a) is very large when w_o is changing rapidly and b) yields vigorous entrainment when the combustion surface is close to the plume edge. Since acceleration is most rapid and the combustion surface is nearest the plume edge near the pool surface, replacing w_o by $r_c \, dw_o/dz$ in Eqs. (15) and (16) near the surface of a burning pool should lead to predictions consistent with Thomas' observations. Based on the considerations above, I postulate the following entrainment law for fire plumes with low initial momentum:

$$-\lim_{r\to\infty} \rho u r = \alpha[\rho_o/\rho_\infty]^{n-1/2} \rho_\infty \delta [w_o + (k/\alpha)\eta_c \delta \, dw_o/dz] \tag{17}$$

The quantity k is an empirical constant and η_c is the value of η on the combustion surface. The factor η_c in Eq. (17) ensures an asymptote to the Morton law (16) after combustion is complete, i.e., when $\eta_c = 0$ [note that, if a top-hat density profile is used, $\hat{\delta} = \delta(\rho_\infty/\rho_o)^{1/2}$].

B. Thermochemistry

Following Nielsen and Tao,[4] combustion is idealized to occur over an infinitesimally thin region; thermodynamic equilibrium

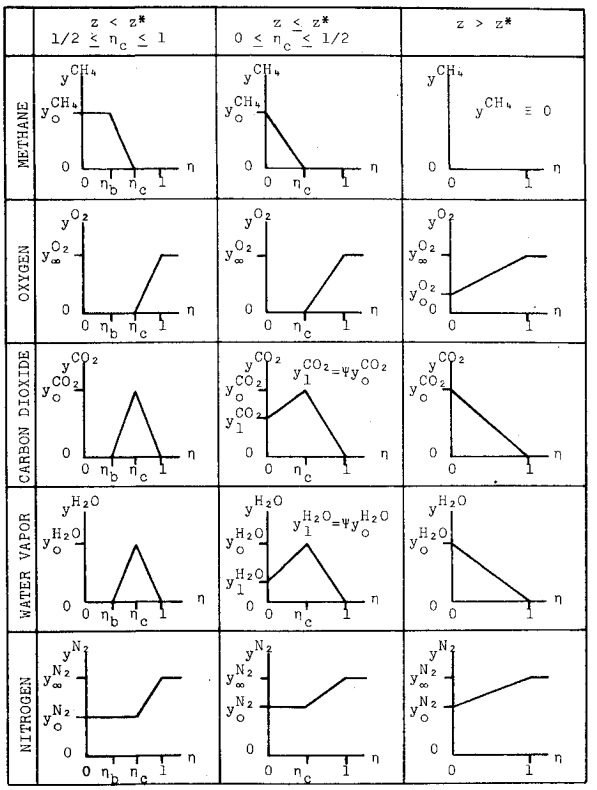

Fig. 1 Mass-fraction profiles; η_c is the combustion-line parameter, $\eta_b = (2\eta_c - 1)$, and $\Psi = \eta_b/(\eta_c - 1)$.

is assumed and finite-rate effects neglected. Hence, whenever oxygen and fuel ignite, an instantaneous reaction occurs. For simplicity, an idealized natural-gas burning reaction is assumed in formulating the model, namely†

$$CH_4 + 2O_2 + 7.52N_2 = CO_2 + 2H_2O + 7.52N_2 \tag{18}$$

Equation (11), the conservation of species equation, contains the average chemical production rate, ϕ_i, defined as

$$\phi_i = \int_0^\infty P_i r \, dr \tag{19}$$

Now, since oxygen is a limiting reagent in the reaction Eq. (18), necessarily

$$\frac{\phi_{CH}}{-M_{CH}} = \frac{\phi_{O_2}}{-2M_{O_2}} = \frac{\phi_{CO_2}}{M_{CO_2}} = \frac{\phi_{H_2O}}{2M_{H_2O}} \tag{20}$$

Contrasting with Nielsen and Tao, molecular weight appears in the denominators of Eq. (20). Molecular weight must be included because the conservation of species equation is written in terms of mass fraction; mistakenly Nielsen and Tao leave out molecular weight in their formulation, an approach which is valid only if mole fractions are used. Hence, the average chemical production rates can all be related to the average production rate of oxygen, i.e.,

$$\begin{aligned} \phi_{CH} &= \tfrac{1}{4}\phi_{O_2}, \qquad \phi_{CO_2} = -\tfrac{11}{16}\phi_{O_2} \\ \phi_{H_2O} &= -\tfrac{9}{16}\phi_{O_2}, \qquad \phi_{N_2} = 0 \end{aligned} \tag{21}$$

where the last of Eqs. (21) expresses the fact that atmospheric nitrogen does not participate in the reaction.

Mass-fraction profiles are required in order to determine ϕ_{O_2}, which will be needed to evaluate the enthalpy integral in the energy equation (13). Nielsen and Tao use top-hat profiles which is equivalent to assuming that oxygen entrained at a given height reacts at that height. Thus, until all fuel is consumed, the oxygen mass fraction inside the plume is zero, with burning occurring

† For general applications, some account should be taken of carbon particle (soot) formation and CO_2 dissociation.

near the plume edge. Their model overestimates oxygen consumption (and hence, ϕ_{O_2}) as evidenced by their computing a peak temperature near the adiabatic flame temperature, even though the flame loses energy through thermal radiation.

To obtain more realistic temperatures, this study's mass-fraction profiles allow for unreacted oxygen between the combustion surface and the fire-plume edge. Figure 1 shows assumed mass-fraction profiles; all curves consist of straight-line segments. Combustion surface location is $\eta = \eta_c(z)$ and z^* denotes the altitude at which all fuel has reacted so that $\eta_c(z^*) = 0$. The profiles exhibit several important features of a diffusion flame. For example, comparison of oxygen and methane mass-fraction profiles shows that fuel and oxygen are nowhere coexistent, thus precluding premixed reactants. Also, products of combustion (carbon dioxide and water vapor) reach maximum concentrations near the combustion surface, where they are being produced, while nitrogen is distributed throughout the flame, as a result of turbulent mixing.

A sufficient number of algebraic equations can be obtained to solve for the several profile functions, i.e., $\eta_c(z)$, $y_o^{CH}(z)$, etc, by using the fact that the sum of mass fractions must everywhere be unity; algebraic details have been presented by Wilcox.[8] Then, using conservation of species, the functions are expressed in terms of $\rho_\infty w_o \delta^2$; for example, the combustion line parameter, η_c, is shown in Fig. 2 as a function of the nondimensional mass-flux reciprocal $m^{-1} = \dot{m}/\rho_\infty w_o \delta^2$ where $\dot{m}$ is the value of $\rho_\infty w_o \delta^2$ at $z = 0$. The two following equations implicitly define η_c as a function of m^{-1}:

$$y_\infty^{O_2}[m^{-1} - (1+\eta_c+\eta_c^2)/3][1+3\eta_c^3] + 4[1-2\eta_c^3]m^{-1} = 0 \quad \text{for } 0 \leqq \eta_c \leqq 1/2 \tag{22}$$

$$y_\infty^{O_2}[m^{-1} - (1+\eta_c+\eta_c^2)/3][5-19\eta_c+29\eta_c^2] + 24m^{-1}\eta_c(1-\eta_c) = 0 \quad \text{for } 1/2 \leqq \eta_c \leqq 1 \tag{23}$$

The average oxygen production rate follows from inserting the assumed oxygen mass-fraction profile in Eq. (11) and performing the indicated integration, wherefore

$$\phi_{O_2} = -\tfrac{1}{2} y_\infty^{O_2} H(z^*-z)(d/dz)[\rho_\infty w_o \delta^2(1+\eta_c+\eta_c^2)/3] \tag{24}$$

The Nielsen-Tao formulation yields Eq. (24) with $\eta_c = 1$. Hence, the production rate will be as much as a factor of three smaller in the present model than that predicted by the Nielsen-Tao model.

Specifying mass-fraction profiles and chemical production rates permits evaluation of the enthalpy integral in Eq. (13). Specific heat ratio, γ, is assumed the same for all flame gases. Hence,

$$C_{p_i} = (\gamma/\gamma - 1)(R/M_i) \tag{25}$$

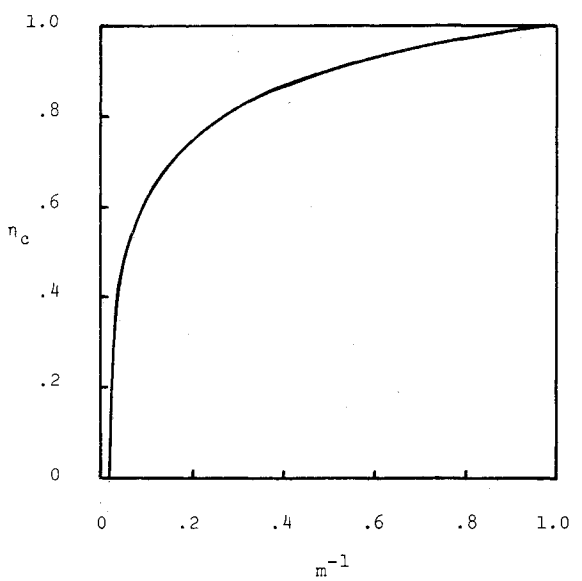

Fig. 2 Combustion line parameter, η_c, as a function of nondimensional mass-flux reciprocal, m^{-1}.

where R is the universal gas constant. Therefore, using Eqs. (5–7, 11, 14, 19, 25), the enthalpy integral becomes

$$d/dz \int_0^\infty \rho w h r\, dr = (d/dz)[\rho_\infty w_o \hat{\delta}^2 C_{p_\infty} T_\infty] + \sum_i [h_i^{(o)} - C_{p_i} T_c][\phi_i + \tfrac{1}{2} y_\infty{}^i (d/dz)(\rho_\infty w_o \delta^2)] \tag{26}$$

Since the heats of formation of O_2 and N_2 are defined to be zero, necessarily

$$\sum_i y_\infty{}^i h_i^{(o)} = 0 \tag{27}$$

Also, noting Eq. (20), there follows

$$\sum_i C_{p_i} \phi_i = (\gamma/\gamma - 1) R \sum_i \phi_i / M_i = 0 \tag{28}$$

Then, denoting the heat of combustion by $\Delta H^{(o)}$,

$$\Delta H^{(o)} = -\sum_i h_i^{(o)} \phi_i / \phi_{O_2} \tag{29}$$

Finally, Eqs. (26–29) are combined and the enthalpy integral is

$$d/dz \int_0^\infty \rho w h r\, dr = \tfrac{1}{2} d/dz[\rho_\infty w_o \hat{\delta}^2 C_{p_\infty} T_\infty] - \tfrac{1}{2} C_{p_\infty} T_c\, d/dz[\rho_\infty w_o \delta^2] - \Delta H^{(o)} \phi_{O_2} \tag{30}$$

Information for closing equation set (5–14) may be summarized as follows. The postulated entrainment law Eq. (17), average oxygen production rate Eq. (24), and enthalpy integral, Eq. (30), can be used to rewrite the conservation of mass, momentum and energy (Eqs. 10, 12, 13) as

$$(d/dz)[\rho_\infty w_o \delta^2] = 2\alpha(\rho_o/\rho_\infty)^{n-1/2} \rho_\infty \delta[w_o + (k/\alpha)\eta_c \delta\, dw_o/dz] \tag{31}$$

$$(d/dz)[\rho_\infty w_o{}^2 \delta^2] = 2\rho_\infty g[\hat{\delta}^2 - \delta^2] \tag{32}$$

$$(d/dz)[\rho_\infty w_o \delta^2 \{C_{p_\infty} T_\infty(\hat{\delta}^2/\delta^2 - 1) + \tfrac{1}{2} w_o{}^2\}] = 2\int_0^\infty Q_R r\, dr - y_\infty{}^{O_2} \Delta H^{(o)} H(z^*-z)(d/dz)[\rho_\infty w_o \delta^2(1+\eta_c+\eta_c^2)/3] - \rho_\infty w_o \delta^2[g + C_{p_\infty} dT_\infty/dz] \tag{33}$$

The conservation-of-species, Eq. (11), permits expression of the combustion line parameter, η_c, as the function of $m^{-1} = \dot{m}/\rho_\infty w_o \delta^2$ implicitly defined in Eqs. (22) and (23) and depicted in Fig. 2.

Two additional things are required for closure, namely, specification of a density profile (in order to relate $\hat{\delta}$ and δ) and evaluation of the radiation-heat-loss term, $\int_0^\infty Q_R r\, dr$. Thermal radiation is discussed in the next section. The density profile is

$$\rho(\eta, z) = \begin{cases} \rho_o(z), & 0 \leqq \eta \leqq \tilde{\eta} \\ \rho_\infty(z) + [\rho_o(z) - \rho_\infty(z)][(1-\eta)/(1-\tilde{\eta})], & \tilde{\eta} \leqq \eta \leqq 1 \\ \rho_\infty(z), & \eta > 1 \end{cases} \tag{34}$$

where $\tilde{\eta}$ is defined by

$$\tilde{\eta} = \eta_c + \zeta(1 - \rho_o/\rho_\infty)(1-\eta_c) \tag{35}$$

and ζ is an empirical constant within the range $0 < \zeta \leqq 1$. The physical fire-plume radius, $\hat{\delta}$, can now be related to the scaled radius, δ, by using the density profile, Eq. (34), in evaluating the intergral in Eq. (14), whereby

$$\hat{\delta}^2 = \delta^2 \left\{ \tilde{\eta}^2 + \frac{2(\rho_o/\rho_\infty)(1-\tilde{\eta})}{(1-\rho_o/\rho_\infty)^2} \left[(1-\tilde{\eta})(1-\rho_o/\rho_\infty) - (\tilde{\eta} - \rho_o/\rho_\infty) \log \frac{\rho_o}{\rho_\infty} \right] \right\} \tag{36}$$

C. Thermal Radiation

To complete the set of fire-plume equations (5, 6, 22, 23, 31–33, 36) derived in the preceding sections, the radiation-heat-loss term, $\int_0^\infty Q_R r\, dr$, must be evaluated. The classical approach of assuming the flame to be optically thick in the axial direction is used in the fire model; radiative transport thus becomes a local phenomenon. To make the flame model applicable to clean-burning fires, for which finite radiation mean-free path is typical, the present approach uses the Kármán-Pohlhausen integral method to solve the radiative heat transfer equation; radiating gases are represented as nongray radiators by using Edwards'[9] exponential-band model for mass absorptivities. Highlights of the

approach are given in this section; complete details have been presented by Wilcox.[8]

First, note that Q_R is minus the divergence of the radiation-heat-flux vector, $\mathbf{q}$; hence, the radiation-heat-loss term is

$$\int_0^\infty Q_R r\,dr = -\lim_{r\to\infty} rq_r - \frac{d}{dz}\int_0^\infty q_z r\,dr \tag{37}$$

where q_r and q_z are the radial and axial components, respectively, of $\mathbf{q}$. To compute the radiation-heat-flux vector, the local radiation field intensity, I_ν, must be integrated over wave number, ν, and solid angle, Ω, according to the following expression:

$$\mathbf{q} = c\int_0^\infty \int\!\!\int_{+\pi} I_\nu \mathbf{n}\,d\Omega\,d\nu \tag{38}$$

where c is the speed of light and $\mathbf{n}$ is a unit vector along a line of sight. The radiation field intensity satisfies the radiative transfer equation, which is

$$\mathbf{n}\cdot\nabla I_\nu = \rho K_\nu(B_\nu - I_\nu) \tag{39}$$

where the effects of scattering and induced emission have been neglected. The quantity K_ν is mass absorptivity and is given in terms of the mass absorptivities of the various radiating species, K_{ν_i}, by

$$K_\nu = \sum_i y^i K_{\nu_i} \tag{40}$$

Assuming radiative equilibrium, the source term B_ν is the Planck radiation function defined by

$$B_\nu = (2h\nu^3/c^2)(1/\exp(h\nu/kT) - 1) \tag{41}$$

where h and k are Planck's constant and Boltzmann's constant, respectively.

In the most general case, the integral in Eq. (38) will extend over a range of altitudes so that the coupled flame-radiation equations are a set of integro-differential equations. However, the mathematics simplifies considerably if the flame is optically thick in the direction of its symmetry axis, as is generally true for any large diffusion flame. That is, axial radiation heat transfer will occur through the diffusive process of the Rosseland limit.[11] Radiative transfer will thus be an effect localized to a given altitude, whereby the "integro-" aspect is eliminated and the equations of motion are pure differential equations. Furthermore, in the spirit of the shear-column approximations, axial heat diffusion can be neglected so that Eq. (37) simplifies to

$$\int_0^\infty Q_R r\,dr \approx -\hat{\delta} q_r(\hat{\delta}, z) \tag{42}$$

For radiation properties in the radial direction, the wave-number integration in Eq. (38) can be done analytically, for two special limits, namely, the Rosseland (optically thick) limit and the Planck (optically thin) limit.[11] If the flame is optically thick, a perturbation solution of Eq. (39) for $\rho K_\nu \to \infty$ can be obtained. The Rosseland mean-free-path (mfp) evolves as the average mfp for the entire wave-number spectrum, thus obviating dealing with spectral effects. Similarly, for the Planck limit, Eq. (39) permits determining I_ν from a perturbation solution with $\rho K_\nu \to 0$; again, a spectrally averaged mfp, known as the Planck mean-free-path, evolves. Thus, in both the optically thick and thin limits, classical analysis makes it possible to avoid complicated spectral effects.

Neither of these "gray-gas" limits is appropriate for a clean-burning (relatively soot free) fire, however; i.e., there is no spectrally averaged mfp for this case since the gaseous products of combustion radiate in discrete wave number bands with essentially transparent "windows" separating the bands. To account accurately for spectral effects, the approach taken here is the same as in the original fire model[8]; specifically, Eq. (39) is solved using the Kármán-Polhausen method; Edwards'[9] exponential-band model is used to compute mass absorptivity. Edwards' model approximates K_{ν_i} with an analytical function of wave number, temperature and pressure; several empirical parameters appear in the expression for K_{ν_i} which must be determined experimentally for each radiating specie. Expressions for CH_4, CO_2, H_2O and CO are tabulated by Edwards[9] and Wilcox.[8]

Derivation of an expression for the quantity $q_r(\hat{\delta}, z)$ is extremely involved and, since complete details have been given by Wilcox,[8] the derivation will not be repeated here. Utilizing the fire-plume's symmetry in the derivation, the following expression results for $q_r(\hat{\delta}, z)$:

$$q_r(\hat{\delta}, z) = 4c\int_0^\infty \int_0^{\hat{\delta}} \rho K_\nu B_\nu \int_0^{\sin^{-1}(r/\hat{\delta})} \cos\theta \times \frac{[W_o(\tau_\nu - t_\nu) + W_o(\tau_\nu + t_\nu)]}{(r^2 - \hat{\delta}^2\sin^2\theta)^{1/2}}\,d\theta\,r\,dr\,d\nu + 4c\int_0^\infty B_\nu(T_\infty, \nu)\int_0^{\pi/2} V_o(2\tau_\nu)\cos\theta\,d\theta\,d\nu - \sigma T_\infty{}^4 \tag{43}$$

where σ is the Stefan-Boltzmann constant.

The quantities $t_\nu(r,\theta)$ and $\tau_\nu(\theta)$ are optical thickness functions given by

$$t_\nu(r,\theta) = \int_{\hat{\delta}\sin\theta}^{r} \frac{\rho K_\nu \tilde{r}\,d\tilde{r}}{(\tilde{r}^2 - \hat{\delta}^2\sin^2\theta)^{1/2}} \tag{44}$$

and

$$\tau_\nu(\theta) = t_\nu(\hat{\delta}, \theta) \tag{45}$$

The functions $W_o(x)$ and $V_o(x)$ are defined in terms of the modified Bessel functions of the second kind, $K_o(x)$ and $K_1(x)$, as

$$W_o(x) \equiv x\left[K_1(x) + \int_0^x K_o(t)\,dt - \pi/2\right] \tag{46}$$

$$V_o(x) \equiv \frac{1}{2}\left[\int_0^x K_o(t)\,dt + \pi/2 - xW_o(x)\right] \tag{47}$$

Equations (40–47) taken together with appropriate exponential-band-model expressions for the K_{ν_i} give the required formula for the radiation-heat-loss term needed to close the flame-radiation equations.

D. Nondimensional Forms and Initial Conditions

The flame-radiation equations are analyzed conveniently in nondimensional form; hence, the following non-dimensional quantities are introduced:

$$\bar{z} = z/L, \quad \bar{r} = r/\alpha L, \quad \bar{\Delta} = \hat{\delta}/\alpha L, \quad \bar{\rho} = \rho_o/\rho_\infty$$
$$\bar{\delta} = \delta/\alpha L\bar{\rho}^{1/2}, \quad \bar{w} = w_o/(gL)^{1/2}, \quad \bar{T} = T/T_R, \quad \bar{K}_\nu = \rho_o \alpha L K_\nu$$
$$\bar{q}_r = q_r/\sigma T_R{}^4, \quad \bar{\nu} = \nu/\nu_*, \quad m = \rho_\infty w_o \delta^2/\dot{m} \tag{48}$$

where

$$T_R \equiv -y_\infty{}^{O_2}\Delta H^{(o)}/C_{p_\infty}, \quad \nu_* \equiv kT_R/hc, \quad L \equiv [\dot{m}/\rho_{\infty_o} g^{1/2}\alpha^2]^{2/5} \tag{49}$$

The quantities ρ_{∞_o} and $\dot{m}$ are the values of ρ_∞ and $\rho_\infty w_o \delta^2$ at $z = 0$. In terms of these variables, the equations of motion become

$$dm/d\bar{z} = 2(\rho_\infty/\rho_{\infty_o})\bar{\rho}^n\bar{\delta}[\bar{w} + k\eta_c\bar{\rho}^{1/2}\bar{\delta}\,d\bar{w}/d\bar{z}] \tag{50}$$

$$d(m\bar{w})/d\bar{z} = 2(\rho_\infty/\rho_{\infty_o})(\bar{\Delta}^2 - \bar{\rho}\bar{\delta}^2) \tag{51}$$

$$d/d\bar{z}\{m[\bar{T}(\bar{\rho}\bar{\Delta}^2/\bar{\delta}^2 - 1) + \tfrac{1}{2}B\bar{w}^2]\} = -2R_d\bar{\Delta}\bar{q}_r + H(\bar{z}^* - \bar{z})d/d\bar{z}[(1 + \eta_c + \eta_c{}^2)m/3] - m[d\bar{T}_\infty/d\bar{z} + B] \tag{52}$$

$$\bar{\Delta}^2 = \bar{\rho}\bar{\delta}^2\left\{\tilde{\eta}^2 + 2\frac{\bar{\rho}(1-\tilde{\eta})}{(1-\rho)^2}[(1-\tilde{\eta})(1-\bar{\rho}) - (\tilde{\eta} - \bar{\rho})\log\rho]\right\} \tag{53}$$

with

$$\tilde{\eta} = \eta_c + \zeta(1-\bar{\rho})(1-\eta_c) \tag{54}$$

The nondimensional parameters B and R_d are defined by the following expressions:

$$B \equiv gL/C_{p_\infty}T_R \tag{55}$$

$$R_d \equiv \alpha L^2\sigma T_R{}^3/\dot{m}C_{p_\infty} \tag{56}$$

The quantity B is a measure of the effects of atmospheric stratification; if the atmosphere follows the adiabatic lapse rate, $B = -d\bar{T}_\infty/d\bar{z}$, so that the last term on the right-hand side of Eq. (52) vanishes. The parameter R_d gives an order-of-magnitude

estimate of the ratio of heat radiated to energy released by chemical reaction.

The nondimensional radiation-heat-flux vector is:

$$\bar{q}_r = \frac{60}{\pi^5}\bar{\delta}^2 \int_0^\infty \eta\, d\eta \int_0^1 \frac{\bar{\nu}^3 \bar{K}_\nu\, d\bar{\nu}}{\exp(\bar{\nu}/\bar{T})-1} \int_0^{\sin^{-1}\left[\frac{\bar{r}(\eta)}{\bar{\Delta}}\right]} \times$$

$$\frac{[W_o(\tau_\nu - t_\nu) + W_o(\tau_\nu + t_\nu)]\cos\theta\, d\theta}{(\bar{r}^2(\eta) - \bar{\Delta}^2 \sin^2\theta)^{1/2}} + \frac{60}{\pi^5}\int_0^\infty \frac{\bar{\nu}^3}{\exp(\bar{\nu}/\bar{T}_\infty)-1} \times$$

$$\int_0^{\pi/2} V_o(2\tau_\nu)\cos\theta\, d\theta\, d\bar{\nu} - \bar{T}_\infty{}^4 \qquad (57)$$

where $\bar{r}(\eta)$ is obtained by integrating Eq. (8); the optical thickness functions t_ν and τ_ν are given by

$$t_\nu(\eta,\theta) = \bar{\delta}^2 \int_{\eta_m(\theta)}^{\eta} \frac{\bar{K}_\nu\, \eta\, d\eta}{(\bar{r}^2(\eta) - \bar{\Delta}^2 \sin^2\theta)^{1/2}} \qquad (58)$$

$$\tau_\nu(\theta) = t_\nu(1,\theta) \qquad (59)$$

with $\eta_m(\theta)$ implicitly defined by the relation

$$\bar{r}[\eta_m(\theta)] = \bar{\Delta}\sin\theta \qquad (60)$$

Local plume temperature needed in evaluating integrals in Eq. (57) is obtained from the equation of state, which is

$$\bar{\rho}\bar{T}\sum_i y^i/M_i = \bar{T}_\infty \qquad (61)$$

Equation set (22, 23, 50–61), plus a) appropriate expressions for the mass-fraction profiles depicted in Fig. 1 (see Wilcox[8]) and b) Edwards' mass absorptivity formulas[9] is a first-order nonlinear set of ordinary differential equations. To obtain a well posed initial-value problem conditions at $z = 0$ must be specified; integration can then proceed to any desired altitude using the standard Runge-Kutta technique. For a pool fire, only two things need be specified at $z = 0$, namely, temperature, $T(0)$, and initial plume radius, $\hat{\delta}(0)$. If the pool radius is R and the initial fire-plume temperature is T_o, then

$$\bar{\Delta}(0) = R/\alpha L \qquad (62)$$

$$\bar{T}(0) = T_o/T_R \qquad (63)$$

Initial values for all other quantities follow from Eqs. (62) and (63) by using the equation of state and the fact that $m(0) = 1$ by definition.

Four empirical parameters appear in the flame-radiation equations, namely, α, n, k, and ζ. The first three parameters appear in the entrainment law while ζ is a density-profile parameter; α and n are presumed to be the same quantities used by Taylor and Morton so that only two new empirical constants, k and ζ, have been introduced. Values of α and n used in the present study are

$$\alpha = 1/10, \quad 0 \leqq n \leqq 1/2 \qquad (64)$$

Numerical experimentation (Sec. 3) indicates that k and ζ should be given by

$$k = 1/10, \quad \zeta = 1 \qquad (66)$$

III. Applications

A computer program, called the LNG Flame Code,[12] has been devised which can be used to solve the flame-radiation equations of Sec. II. The code has been used to predict properties of fires above LNG pools of various radii. Computational results and comparisons with experimental data for flame-height and spectral-radiation properties follow.

Table 1 presents calculated flame-height-to-diameter ratio, L^*/D, for various LNG pool diameters, D. Mass flux, $\dot{m}$, for each case is indirectly specified by giving LNG pool surface-recession (boiloff) rate, $\dot{h}$. Values of n and T_o have little effect on flame-model predictions; results summarized in the table have been obtained with $n = 0$ (Taylor's value) and $T_o = 878°R$ (corresponding to an initial combustion surface temperature of 1463°R, the autoignition temperature of methane). Thomas'[6] criterion has been used to locate flame top (i.e., the point at which the temperature on the axis drops to 1440°R). L^*/D is

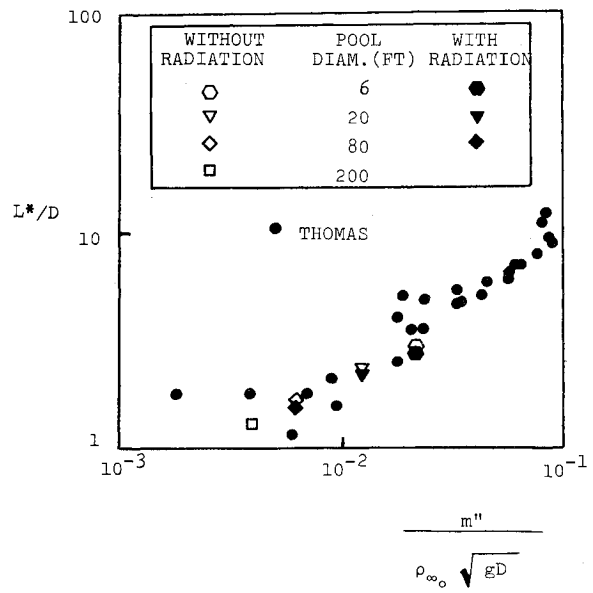

Fig. 3 Comparison of calculated flame-height-to-diameter ratio with Thomas' flame data.

shown in Fig. 3 as a function of initial mass flux per unit area, $m' = 4\dot{m}/D^2$; calculated ratios are consistent with Thomas' data. The new entrainment law has a pronounced effect; calculations with the Morton entrainment law ($k = 0$, $n = 1/2$) show an increase in L^*/D of about a factor of five.[8] Thus, the present model is clearly more accurate.

A measure of the effect of thermal radiation on flame height is provided by comparing corresponding L^*/D calculated with and without thermal radiation. Inspection of Table 1 shows that thermal radiation reduces L^*/D by about 4%. Hence, thermal radiation is predicted to be a passive mechanism in determining the size of a large diffusion flame, wherefore flame height can be predicted accurately without including radiation effects.

Computed L^*/D values would at first appear inconsistent with recent experimental observations for large LNG fires[13] which indicate larger L^*/D for 20 and 80 ft-diam LNG pools. However, the difference is attributable to the tremendous amount of swirl observed in the experimental tests, an effect which has been neglected in the calculations and which increases flame height. However, agreement between computed L^*/D and Thomas' data is a good measure of the present flame-model's accuracy since Thomas' data have been accumulated for a variety of large fires having typically only a modest amount of swirl.

Table 1 LNG Flame code test cases

D (ft)	$\dot{h}$ (in./min)	Radiation	L^*/D
6	0.6	*No*	3.00
6	0.6	*Yes*	2.87
20	0.6	*No*	2.30
20	0.6	*Yes*	2.20
80	0.6	*No*	1.66
80	0.6	*Yes*	1.59
200	0.6	*No*	1.29

Since all gaseous species present in the flame which emit thermal radiation are described as realistic nongray radiators, the flame model can be used to calculate spectral distribution of the radiation-heat-flux vector, $\mathbf{q}_\nu$. Figure 4 presents a comparison of the computed radial component of $\mathbf{q}_\nu$ with experimental data[14] for a 6-ft-diam LNG pool fire; the curve shown in the figure has been computed at a distance approximately one pool diameter above the LNG pool. Two primary absorption bands ($2.7\mu H_2O$ and $4.3\mu CO_2$) are also shown in the figure.

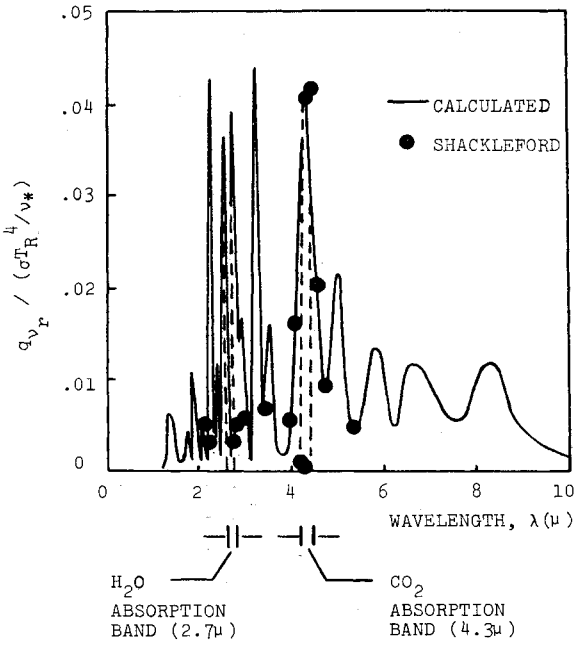

Fig. 4 Comparison of computed and experimentally measured spectral variations of the radiation-heat-flux vector for a flame above a pool of liquefied natural gas; LNG pool diameter, $D = 6$ ft.

Note that the experimental data are actually for the quantity $\int_0^z q_{\nu_r} dz$, which is not conveniently obtained from LNG-Flame-Code output. Hence, the experimental data have been scaled to match the numerical data near the peak at 4μ. Such a scaling is reasonable since these quantities are expected to be proportional. All details, including fine-scale structure appear to be well represented by the flame model.

IV. Summary and Conclusions

Although LNG pool-fire data are sparse, these data do indicate the two primary objectives have been achieved in developing the diffusion-flame model presented in Sec. II. Specifically, the model's applicability extends beyond that of other models in two respects. First, the model applies to fires having low initial momentum as evidenced by accurate prediction of flame height-to-diameter ratio for pool fires. Second, spectral radiation properties of a clean-burning natural-gas fire can be accurately predicted as shown by Fig. 4. Even more significantly, although the model has been formulated and tested specifically for LNG pool fires, the model has been developed using general methodology. By using an appropriate chemical reaction and mass-absorptivities, the formulation applies to any fire having low initial momentum and nongray thermal radiation.

References

[1] Taylor, G. I., Morton, B. R., and Turner, J. S., "Turbulent Gravitational Convection from Maintained and Instantaneous Sources," *Proceedings of the Royal Society (London)*, Ser. A, Vol. 234, 1956, pp. 1–23.

[2] Murgai, M. P. and Emmons, H. W., "Natural Convection Above Fires," *Journal of Fluid Mechanics*, Vol. 8, 1960, pp. 611–624.

[3] Murgai, M. P., "Radiative Transfer Effects in Natural Convection Above Fires," *Journal of Fluid Mechanics*, Vol. 12, 1962, pp. 441–448.

[4] Nielsen, H. J. and Tao, L. N., "The Fire Plume Above a Large Free-Burning Fire," *Tenth Symposium (International) on Combustion*, The Combustion Institute, Pittsburgh, Pa., 1965, pp. 965–972.

[5] Morton, B. R., "Modeling Fire Plumes," *Tenth Symposium (International) on Combustion*, The Combustion Institute, Pittsburgh, Pa., 1965, pp. 973–982.

[6] Thomas, P. H., Baldwin, R. and Heselden, A. J. M., "Buoyant Diffusion Flames: Some Measurements of Air Entrainment, Heat Transfer, and Flame Merging," *Tenth Symposium (International) on Combustion*, The Combustion Institute, Pittsburgh, Pa., 1965, pp. 983–996.

[7] Smith, R. K., "Radiation Effects on Large Fire Plumes," *Eleventh Symposium (International) on Combustion*, The Combustion Institute, Pittsburgh, Pa., 1967, pp. 507–515.

[8] Wilcox, D. C., "Non-Gray Thermal Radiation from a Flame Above a Pool of Liquid Natural Gas," Catalog No. M19714, 1971, American Gas Association, Inc., Arlington, Va.

[9] Edwards, D. K., Glassen, L. K., Hauser, W. C., and Tuchscher, J. S., "Radiation Heat Transfer in Nonisothermal Nongray Gases," *Transactions of the ASME, Journal of Heat Transfer*, Vol. 89, 1967, pp. 219–229.

[10] Schlichting, H., *Boundary Layer Theory*, 4th ed., McGraw-Hill, New York, 1960, p. 243.

[11] Pai, Shih-I, *Radiation Gasdynamics*, Springer-Verlag, Berlin, 1966.

[12] Wilcox, D. C., "A User's Guide for the LNG Flame Code," Rept. DCW-TR-02-01, 1974, DCW Industries, Sherman Oaks, Calif.

[13] "Radiation from LNG Fires," Rept. 73854, 1973, Arthur D. Little, Inc., Cambridge, Mass.

[14] Shackleford, W., "Results of Spectroscopic Measurements on Six Foot Diameter LNG Pool Fires at Capistrano Test Site," IOC 4360.3.72-050, 1972, TRW Systems Group, Redondo Beach, Calif.